Ghost imaging with a single detector

Yaron Bromberg, Ori Katz, and Yaron Silberberg*
Department of Physics of Complex Systems, The Weizmann Institute of Science, Rehovot 76100, Israel
(Received 18 December 2008; published 19 May 2009)

We experimentally demonstrate pseudothermal ghost imaging and ghost diffraction using only a single detector. We achieve this by replacing the high-resolution detector of the reference beam with a computation of the propagating field, following a recent proposal by Shapiro [Phys. Rev. A **78**, 061802(R) (2008)]. Since only a single detector is used, this provides experimental evidence that pseudothermal ghost imaging does not rely on nonlocal quantum correlations. In addition, we show the depth-resolving capability of this ghost imaging technique.

DOI: 10.1103/PhysRevA.79.053840 PACS number(s): 42.50.Ar, 42.30.Va, 42.50.Dv

Ghost imaging (GI) has emerged a decade ago as an imaging technique which exploits the quantum nature of light. This field has attracted great interest, and has been in the focus of many studies since. In GI an object is imaged even though the light which illuminates it is collected by a single-pixel detector which has no spatial resolution (a bucket detector). This is done by using two spatially correlated beams. One of the beams illuminates the object, and the photons transmitted by the object are collected by the bucket detector. The other beam impinges on a multipixel detector [e.g., a charge-coupled device (CCD) camera], without ever passing through the object (the reference beam). Nevertheless, by correlating the intensities measured by the bucket detector with the intensities of each pixel in the multipixel detector, an image of the object is reconstructed [1]. In a similar fashion, the diffraction pattern of the object can also be obtained ["ghost diffraction" (GD)]. In the first demonstrations of GI and GD the two beams were formed from a stream of entangled photons [2,3]. The reconstruction of the image was attributed to the nonlocal quantum correlations between the photon pairs. Challenging this interpretation, Bennink *et al.* [4] demonstrated GI using two classically correlated beams, and triggered an ongoing effort to clarify the role of entanglement in GI and GD [5–14]. It was soon discovered that many of the features obtained with entangled photons are reproduced with a classical pseudothermal light source [7–9]. However, the nature of the spatial correlations exhibited with a pseudothermal source, and whether they can be interpreted as classical intensity correlations [1,11,13] or are fundamentally nonlocal quantum correlations [10,15], is still under debate.

In this paper we experimentally study *computational ghost imaging*, a novel ghost imaging technique recently proposed by Shapiro [16]. In this technique the multipixel detector is replaced with a "virtual detector," by calculating the propagation of the field of the reference beam. The image is reconstructed by correlating the calculated field patterns with the measured intensities at the object arm. In addition, we propose and demonstrate computational GD. Our measurements show that pseudothermal GI and GD can be performed with only one beam and one detector. As noted by Shapiro [16], this proves that pseudothermal GI cannot possibly depend on nonlocal quantum correlations. We also demonstrate scanningless three-dimensional (3D) sectioning capability of this technique.

Computational GI can be considered as a variant of the standard two-detector pseudothermal GI. In pseudothermal GI, a spatially incoherent beam is generated by passing a laser beam through a rotating diffuser [Fig. 1(a)]. The beam is then split on a beam splitter, generating the two spatially correlated beams required for GI. The essence of computational GI is to replace the rotating diffuser with a computer-controlled spatial light modulator (SLM), which serves as a controlled phase mask for the spatial phase of the light field, $\varphi(x,y)$ [Fig. 1(b)]. A spatially incoherent beam is generated by applying pseudorandom phase patterns $\varphi_r(x,y)$ on the SLM. Since for each phase realization r the controlled phase pattern is known, one can evaluate the field right after the

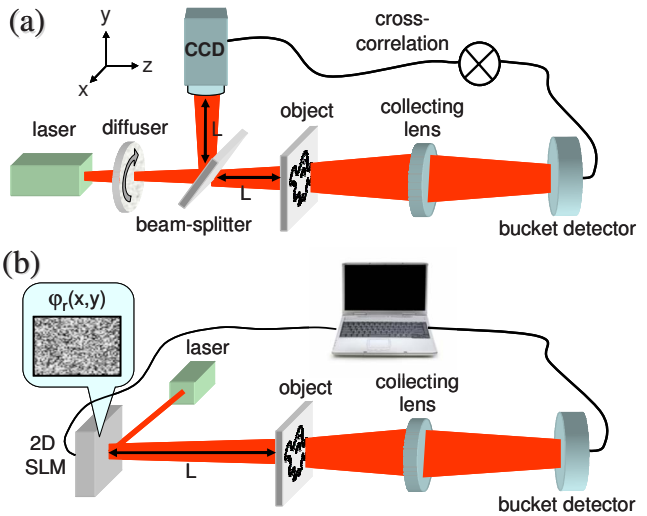

FIG. 1. (Color online) Experimental setups for ghost imaging. (a) The standard pseudothermal two-detector setup, where a ghost image of the object is obtained by correlating the pseudothermal field measured by a CCD with the intensity measured by a bucket detector. (b) The computational single-detector setup used in this work. A pseudothermal light beam is generated by applying controllable phase masks $\varphi_r(x,y)$ with a spatial light modulator (SLM). The object image is obtained by correlating the intensity measured by the bucket detector with the *calculated* field at the object plane.

*yaron.silberberg@weizmann.ac.il

SLM, $E_r(x,y,z=0)=E^{(in)}e^{i\varphi_r(x,y)}$ (where $E^{(in)}$ is the incident field on the SLM). Knowing $E_r(x,y,z=0)$, the field at any distance z from the SLM can be computed using the Fresnel-Huygens propagator:

$$E_r(x,y,z)=\frac{e^{i\lambda z}}{i\lambda z}\int d\xi d\eta E_r(x-\xi,y-\eta,0)e^{i(\pi/\lambda z)(\xi^2+\eta^2)}, \tag{1}$$

where λ is the wavelength of the source. In order to reconstruct the transmission function of an object, $T(x,y)$, placed at $z=L$, the *computed* intensity patterns at the object plane, $I_r=|E_r(x,y,z=L)|^2$, are cross-correlated with the intensities *measured* by the bucket detector placed behind the object, $B_r=\int dxdy I_r(x,y,L)T(x,y)$:

$$G(x,y)\equiv\frac{1}{N}\sum_{r=1}^{N}(B_r-\langle B\rangle)I_r(x,y)=\langle BI(x,y)\rangle-\langle B\rangle\langle I(x,y)\rangle, \tag{2}$$

where $\langle\cdot\rangle\equiv\frac{1}{N}\Sigma_r\cdot$ denotes an ensemble average over N phase realizations. Intuitively, one can see that the image is obtained by summing the calculated intensities I_r with the appropriate weights B_r. The larger the overlap between the generated intensity pattern and the transmission object is, the higher is the intensity measured by the bucket detector B_r, and thus the calculated $I_r(x,y)$ is summed with a larger weight. It is important to note that in conventional GI the object is also reconstructed according to Eq. (2). The only difference is that here $I_r(x,y,z=L)$ are *computed*, whereas in conventional GI I_r are obtained by measuring the intensities at the reference arm using a multipixel detector placed at a specific distance $z=L$. Thus, similar to what is well known for conventional GI, one can show that $G(x,y)$ is given by the transmission function of the object convolved with the coherence function of the field at the plane of the object [1,13]. The resolution of the reconstructed object is therefore limited by the coherence area of the field at the object plane.

To demonstrate computational GI experimentally, we have constructed the setup presented in Fig. 1(b). The setup is based on a two-dimensional phase-only liquid crystal on silicon spatial-light modulator (LCOS-SLM, Holoeye HEO1080P), with 1080×1920 addressable 8×8 μm^2 pixels. The computer-controlled 2D-SLM is illuminated by a cw helium-neon laser, which produces a Gaussian beam with a waist of $w_0=740$ μm on the 2D-SLM plane. A 2×2 cm^2 object (transmission plate) is placed at distance $L=84$ cm from the SLM, and a lens collects the transmitted light onto the bucket detector. In each realization a mask of 300×300 random phases is sent to the SLM, where each phase is realized by 3×3 SLM pixels. The reconstructed image using 16 000 realizations is shown in Fig. 2(a), displaying the accurate reconstruction of the object transmission $T(x,y)$ [Fig. 2(a), inset]. This experimental result cannot be attributed to nonlocal quantum correlations, since only a single detector was used. We note that one can reconstruct an object placed at any distance L from the source, in both the near- and far-field zones, as long as the field at the object plane can be calculated using Eq. (1). This is demonstrated below, with an object placed at $L=11$ cm.

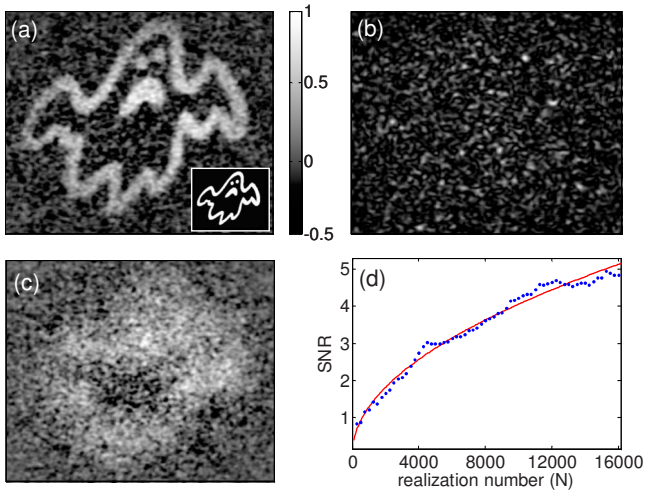

FIG. 2. (Color online) Computational ghost image reconstruction of a 2×2 cm^2 transmission mask placed at $L=84$ cm. (a) Reconstructed image at the object plane, obtained with 16 000 realizations. The inset shows the transmission mask. (b) A calculated intensity pattern of a single phase realization. The resolution of the reconstruction in (a) is dictated by the speckle size. (c) Reconstructed out-of-focus image, at a different z plane ($L=15$ cm), demonstrating the depth-resolving capabilities of the computational method. (d) Measured signal-to-noise ratio (SNR) of the reconstructed image as a function of the number of realizations (blue dots). The theoretical line depicts $\sqrt{N}$ dependence.

An intensity pattern calculated from a *single* realization is shown in Fig. 2(b), revealing the speckle field that impinges on the object for this specific realization of random phases [17]. Reconstruction of an image at a z plane different from the actual location of the object results in an out-of-focus image of the object, indicating the depth-resolving capabilities of computational GI [Fig. 2(c)]. This is analogous to scanning the z position of the multipixel detector in conventional GI, but is performed here for all z locations simultaneously, without the need for additional measurements. Thus, one can perform a full three-dimensional reconstruction of the object field, with the only price of executing more calculations. This is further demonstrated below.

Since the computational GI scheme is completely analogous to pseudothermal GI, the two techniques share similar resolution and signal-to-noise ratio (SNR) properties [16–19]. To summarize these, the transverse resolution is determined by the coherence length (speckle size) at the object plane, which is given by the van Cittert–Zernike theorem $\delta x(z)=\lambda z/\pi w_0$. The depth resolution is given by $\delta z(z)=2\pi\delta x^2/\lambda$. For the presented experimental parameters, $\delta x(L=84\text{ cm})=230$ μm and $\delta z(L=84\text{ cm})=50$ cm, in agreement with the experimental results. In pseudothermal GI, the SNR scales as the square root of the ratio of the number of realizations N and the average number of speckles transmitted through the object N_s, $\text{SNR}\propto\sqrt{N/N_s}$ [18,19]. Since N_s is given by the ratio of the object transmissive area to the coherence area, there is a clear trade-off between resolution and SNR. The SNR as a function of the number of

realizations for the reconstructed image in Fig. 2(a) is presented in Fig. 2(d), in agreement with the theoretical prediction. A movie visualizing the image buildup can found in [20].

One of the features in common to ghost imaging with a nonclassical source and a pseudothermal source is the ability to resolve both the object and its diffraction pattern with high resolution. In conventional GD, the diffraction pattern of the object is reconstructed by replacing the bucket detector with a small single-pixel ("pinhole") detector, placed at the Fourier plane of the collecting lens [6,8]. The GD is reconstructed by correlating the intensities measured by the pinhole detector with the diffraction pattern of the field in the reference arm. The near-field object image (GI) can be reconstructed by correlating the intensities measured by the same pinhole detector, with the image of the speckle field at the object's plane measured by the CCD at the reference arm [21]. Thus, both the near-field object image (GI) and its diffraction pattern (GD) can be obtained by changing only the optical setup at the reference arm. In our single-detector configuration, since the reference arm is virtual, the only required change is in the computational procedure. Therefore, in principle one can perform GI and GD simultaneously, with a single set of measured data (i.e., the intensities measured with the pinhole detector B_r). Both images are reconstructed using Eq. (2), where for GI I_r is computed according to Eq. (1), and for GD I_r is obtained by calculating the Fourier transform (FT) of $E_r(x,y,z=0)$, $I_r=|FT(E_r(x,y,z=0))|^2$. The intensities measured by a pinhole detector placed on the optical axis are given by $B_r=|\int dxdyE_r(x,y,L)T(x,y)|^2$. We note that by using a pinhole detector instead of a bucket detector, the SNR of the GI is degraded since only a small fraction of the transmitted light is collected.

In order to demonstrate the simultaneous reconstruction of GI and GD, we have placed a double-slit transparency at $L=11$ cm from the SLM and a small pinhole detector at the Fourier plane of the collecting lens (a single 8.6×8.4 μm^2 pixel of a CCD camera). We reconstructed both the double-slit diffraction pattern and its transmission image simultaneously, using the same phase realizations. We used the intensities measured by the pinhole detector for reconstructing the diffraction pattern, and the intensities measured by the bucket detector (summing over the CCD's pixels) for the transmission range. We have also used the pinhole detector to reconstruct both the GD and GI, but with much lower SNR for the latter (not shown).

Figure 3 summarizes the results of the near-field and far-field image reconstructions for the double-slit transparency. An image of the double slit obtained with 8000 realizations is shown in Fig. 3(a). To demonstrate the depth resolution, we show in Fig. 3(b) an out-of-focus image reconstructed at a distance $L=5$ cm. A movie summarizing a computational "virtual focusing" reconstruction process, using the same single set of measurements, can be found in [20]. Comparing the GI and GD results, it is obvious that the product of the resolution of the near-field image (δx) and of the far-field image ($\delta k\sim 1/w_0$) is much smaller than the Fourier limit, i.e., $\delta x\delta k=0.025\ll 0.5$. However, this does not violate the Einstein-Podolsky-Rosen (EPR) bound for classical light, as was previously shown with a pseudothermal source [8].

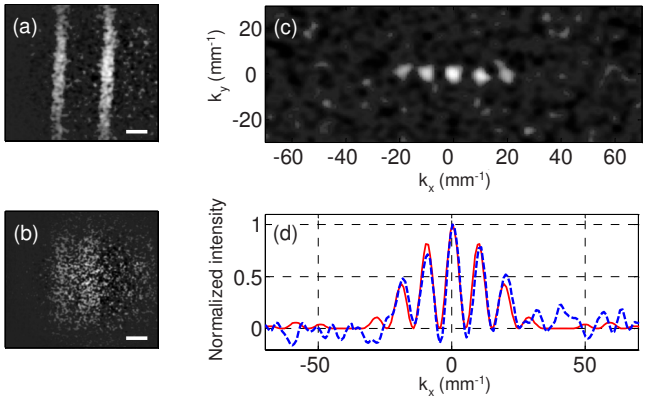

FIG. 3. (Color online) Simultaneous reconstruction of an object and its diffraction pattern, with 8000 realizations. (a) Reconstructed ghost image of a two-slit transmission plate placed at $L=11$ cm. The width of each slit is 170 μm and the separation is 460 μm. The resolution of the image is determined by the speckle size, $\delta x\sim 0.018$ mm. Scale bars indicate 300 μm. (b) An out-of-focus image reconstructed at $L=5$ cm. (c) Ghost diffraction pattern reconstructed using a pinhole detector. The resolution of the diffraction image is $\delta k\sim 1.4$ mm^{-1}, considerably lower than the Fourier limit $\delta x\delta k<0.5$. (d) A cross section of the ghost diffraction pattern shown in (c) (dashed blue line), and the theoretical two-slit diffraction pattern calculated from the dimensions of the double slit (solid red line).

Simultaneous GI and GD cannot be obtained by simply scanning the object with a coherent laser beam [6]. The conditions for performing GI and GD simultaneously with a pseudothermal source depend on the parameters of the object and the source. In order to perform GI of an object with a width W and a minimal feature of size r, placed at a distance L from the source, $\delta x(L)$ must be smaller than r and the speckle field must cover the object: $\lambda L/d\gtrsim W$, where d is the size of the phase elements on the SLM (the coherence length at $L=0$). If one is working in the so-called near-field speckle region ($L\lesssim w_0 d/\lambda$ [22]), the incoming beam diameter should be larger than the object, and the phase element size d should be smaller than r. On the other hand, for GD the maximal k vector reflected from the SLM must be larger than the maximal k vector of the object, i.e., $2\pi/d>2\pi/r$, and proper resolution δk is ensured when $2\pi/w_0<2\pi/W$. Combining the above restrictions for simultaneous GI and GD yields two nontrivial restrictions: (i) $w_0>W$, the size of the beam impinging on the SLM must be larger than the size of the object, and (ii) $d^2/\lambda<L<w_0^2/\lambda$, the object should be placed within the Rayleigh range of the original beam, but beyond the far field of the smallest phase element on the SLM. Under these two conditions, high-resolution near-field and far-field intensity patterns of the object can be obtained, as demonstrated in Fig. 3. Thus, using the Gerchberg-Saxton phase-retrieval algorithm [23], one can reconstruct both the object's transmission amplitude *and* phase. This ability of computational GI might be appealing for phase-sensitive applications.

In conclusion, we have shown that pseudothermal GI can be performed with only a single detector, thus proving that it

does not rely on nonlocal quantum correlations. In addition, we have demonstrated the depth-resolving and diffraction imaging capabilities of this single-detector technique. Finally, we note that in computational GI the main complexity is shifted from the experimental apparatus to the calculation. Thus, it allows for 3D reconstruction by only postprocessing the retrieved data, eliminating mechanical scans. One might consider applying computational GI for other 3D imaging tasks which are not necessarily transmission based. Two examples for such are light detection and ranging (LIDAR) application, and scanningless depth-resolved microscopy using fluorescent probes. Furthermore, the use of a SLM enables the implementation of closed-loop feedback schemes, potentially reducing the number of realizations needed for image reconstruction.

This work was supported by the German-Israel Foundation (GIF) and the Crown Photonic Center.

[1] A. Gatti, M. Bache, D. Magatti *et al.*, J. Mod. Opt. **53**, 739 (2006); A. Gatti, E. Brambilla, and L. A. Lugiato, in *Progress in Optics*, edited by E. Wolf (Elsevier, Amsterdam, 2008), Vol. 51, p. 251.

[2] T. B. Pittman, Y. H. Shih, D. V. Strekalov, and A. V. Sergienko, Phys. Rev. A **52**, R3429 (1995).

[3] D. V. Strekalov, A. V. Sergienko, D. N. Klyshko, and Y. H. Shih, Phys. Rev. Lett. **74**, 3600 (1995).

[4] R. S. Bennink, S. J. Bentley, and R. W. Boyd, Phys. Rev. Lett. **89**, 113601 (2002).

[5] A. Gatti, E. Brambilla, and L. A. Lugiato, Phys. Rev. Lett. **90**, 133603 (2003).

[6] R. S. Bennink, S. J. Bentley, R. W. Boyd, and J. C. Howell, Phys. Rev. Lett. **92**, 033601 (2004).

[7] A. Gatti, E. Brambilla, M. Bache, and L. A. Lugiato, Phys. Rev. Lett. **93**, 093602 (2004).

[8] F. Ferri, D. Magatti, A. Gatti, M. Bache, E. Brambilla, and L. A. Lugiato, Phys. Rev. Lett. **94**, 183602 (2005).

[9] A. Valencia, G. Scarcelli, M. D'Angelo, and Y. Shih, Phys. Rev. Lett. **94**, 063601 (2005).

[10] G. Scarcelli, V. Berardi, and Y. Shih, Phys. Rev. Lett. **96**, 063602 (2006); **98**, 039302 (2007).

[11] A. Gatti, M. Bondani, L. A. Lugiato, M. G. A. Paris, and C. Fabre, Phys. Rev. Lett. **98**, 039301 (2007); A. Pe'er, e-print arXiv:quant-ph/0605131.

[12] L. Basano and P. Ottonello, Opt. Express **15**, 12386 (2007).

[13] B. I. Erkmen and J. H. Shapiro, Phys. Rev. A **77**, 043809 (2008).

[14] R. Meyers, K. S. Deacon, and Y. Shih, Phys. Rev. A **77**, 041801(R) (2008).

[15] Y. Shih, IEEE J. Sel. Top. Quantum Electron. **13**, 1016 (2007); e-print arXiv:0805.1166.

[16] J. H. Shapiro, Phys. Rev. A **78**, 061802(R) (2008).

[17] J. W. Goodman, *Speckle Phenomena in Optics* (Roberts & Co., Greenwood Village, CO, 2007).

[18] A. Gatti, D. Magatti, and F. Ferri, Phys. Rev. A **78**, 063806 (2008).

[19] B. I. Erkmen and J. H. Shapiro, Phys. Rev. A **79**, 023833 (2009).

[20] See EPAPS Document No. E-PLRAAN-79-122905 for movies visualizing the image buildup and the depth-resolving capabilities of computational GI. For more information on EPAPS, see http://www.aip.org/pubservs/epaps.html.

[21] M. Bache, E. Brambilla, A. Gatti, and L. Lugiato, Opt. Express **12**, 6067 (2004).

[22] F. Ferri, D. Magatti, V. G. Sala, and A. Gatti, Appl. Phys. Lett. **92**, 261109 (2008).

[23] R. W. Gerchberg and W. O. Saxton, Optik **35**, 237 (1972).